Abstract

The objective is to solve for the velocity field of several lid driven cavity flow problems. In the first version of the problem a square domain has a lid moving across the top with constant velocity. In the second version of the problem the square domain has a box in the bottom left corner. The solution for the velocity field was required at steady state. In approaching this problem the Navier-Stokes equation was first non-dimensionalized to allow all fluid parameters for the problem (aside from boundary conditions) to be represented simply through the Reynolds number.

The collocated SIMPLE algorithm was used to account for pressure and frictional shear effects and solve the resulting velocity field at steady state. The code was written in FORTRAN and the central difference and upwind schemes were used in the implementation. When comparing schemes it was found that the central difference scheme was less robust than the upwind scheme. The upwind scheme works for all cases but the central difference scheme theoretically fails when the Reynolds number is twice the mesh resolution. The implementation used allowed the central difference scheme to work beyond this but it still failed at low Reynolds numbers.

With regards to the results, gradually increasing Reynolds numbers resulted in the formation of vortices in the bottom two corners of the domain. The vortex formed in the bottom left was larger than the one in the bottom right initially but as Reynolds number increased the bottom right vortex also increased in size and a vortex began forming in the top left corner of the domain. With the presence of a box larger vortices formed in the corners. Also the center of rotation for the vortex in the middle tended towards the geometric center of the domain with higher Reynolds numbers. At higher Reynolds numbers, larger mesh resolutions were required to ensure accurate results. Higher mesh resolutions result in greater accuracy but at the cost of increased computational cost. Higher Reynolds number solutions require tighter convergence criteria, greater mesh resolutions and generally need more iterations in order to yield converged, accurate results. Each of these additional requirements also increases computational cost. As a result the highest Reynolds number with a converged result was 3200 for a mesh size of 120x120. Higher numbers were attempted but time limitations prevented converged results.

1.0 Problem Definition

The objective is to solve for the velocity field of several cavity flow problems. The first is the lid driven cavity flow problem for a square control volume with sides of length, L, fluid of density, ρ, and viscosity, μ. The square control volume has a lid on top that moves with constant speed, U and has solid walls on the other three sides.

The second is a modified version of the cavity flow problem with a solid box in the bottom left corner with sides of length L/3. Figure 1 Cavity Flow Problems illustrates each of the problems.

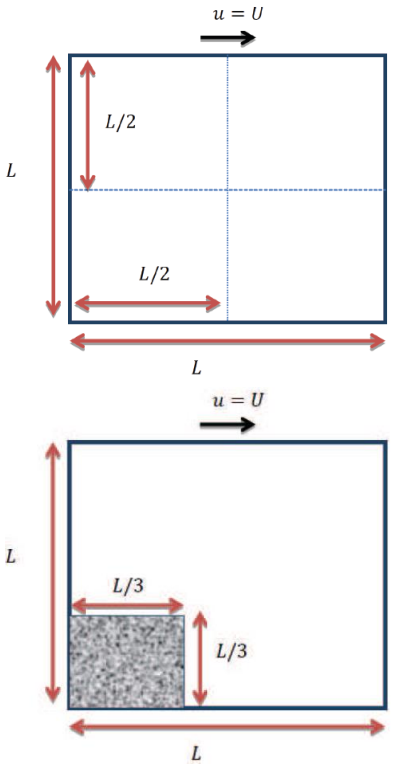

Figure 1 Cavity Flow Problems

The solution to each of these problems will be obtained using the 2D Navier-Stokes equation for incompressible, Newtonian fluids. This equation will be non-dimensionalized and discretized using the collocated SIMPLE algorithm for the upwind, central difference and QUICK schemes.

2.0 Mathematical Formulation

2.1 General Formulation & Non-Dimensionalization

The general form of the transport equation can be written as follows:

$$\frac{\partial}{\partial t}\int_{CV}\rho\vec{u}\,dV+\int_{CV}\vec{\nabla}\cdot(\rho\vec{u}\vec{u})\,dV$$
$$=\int_{CV}\vec{\nabla}\cdot(\mu\vec{\nabla}\vec{u})\,dV+\int_{CV}-\vec{\nabla}P dV$$

Unsteady Term + Convection Term = Diffusion Term + Source Term

Removing the unsteady term & control volume integrals gives:

$$\rho(\vec{u}\cdot\vec{\nabla})\vec{u}=\vec{\nabla}\cdot(\mu\vec{\nabla}\vec{u})+-\vec{\nabla}P$$

Dimensionless variables are substituted into the equation:

$$\vec{u}^*=\frac{\vec{u}}{U}\ \&\ P^*=\frac{P}{\rho U^2}\ \&\ \left.\begin{matrix}x^*=\frac{x}{L}\\ y^*=\frac{y}{L}\end{matrix}\right\}\vec{\nabla^*}=L\vec{\nabla}$$

When simplified the equation becomes:

$$\vec{u}^*\cdot\vec{\nabla^*}\vec{u}^*=-\vec{\nabla^*}P^*+\frac{\mu}{\rho UL}\vec{\nabla^*}\cdot\vec{\nabla^*}\vec{u}^*$$

Since $Re=\frac{\rho UL}{\mu}$, the equation can be written as:

$$\vec{u}^*\cdot\vec{\nabla^*}\vec{u}^*=-\vec{\nabla^*}P^*+\frac{1}{Re}\vec{\nabla^*}\cdot\vec{\nabla^*}\vec{u}^*$$

This evaluates to the non-dimensionalized x-momentum equation:

$$u^*\frac{du^*}{dx^*}+v^*\frac{du^*}{dy^*}=-\frac{dP^*}{dx^*}+\frac{1}{Re}\vec{\nabla^*}\cdot\vec{\nabla^*}u^*$$

Similarly the non-dimensionalized y-momentum equation is:

$$u^*\frac{dv^*}{dx^*}+v^*\frac{dv^*}{dy^*}=-\frac{dP^*}{dy^*}+\frac{1}{Re}\vec{\nabla^*}\cdot\vec{\nabla^*}v^*$$

The continuity equation is also non-dimensionalized:

$$\frac{du^*}{dx^*}+\frac{dv^*}{dy^*}=0$$

Applying the control volume integrals, adding a source term and applying Gauss' Divergence Theorem to the momentum and continuity equations gives:

$$\int_A \vec{u}^* \cdot \overrightarrow{n^*} u^* \, dA = \int_A \frac{1}{Re} \overrightarrow{n^*} \cdot \overrightarrow{\nabla^*} u^* \, dA - \int_{CV} \overrightarrow{\nabla^*} P^* \, dV + \int_{CV} S_u \, dV$$

$$\int_A \vec{u}^* \cdot \overrightarrow{n^*} v^* \, dA = \int_A \frac{1}{Re} \overrightarrow{n^*} \cdot \overrightarrow{\nabla^*} v^* \, dA - \int_{CV} \overrightarrow{\nabla^*} P^* \, dV + \int_{CV} S_u \, dV$$

$$\int_A \frac{du^*}{dx^*} + \frac{dv^*}{dy^*} dA = 0$$

In this equation, $\vec{\nabla} u = \frac{du}{dx}\vec{\imath} + \frac{du}{dy}\vec{\jmath} + \frac{du}{dz}\vec{k}$. However for these two dimensional problems the last term in the gradient is equal to 0, so $\vec{\nabla} u = \frac{du}{dx}\vec{\imath} + \frac{du}{dy}\vec{\jmath}$. For a discrete control volume in the system these equations can be written as:

$$\begin{aligned}\int_{Ae} \vec{u}u \, dA - \int_{Aw} \vec{u}u \, dA + \int_{An} \vec{v}u \, dA - \int_{As} \vec{v}u \, dA \\ = \int_{Ae} \frac{1}{Re}\frac{du}{dx} \, dA - \int_{Aw} \frac{1}{Re}\frac{du}{dx} \, dA \\ + \int_{An} \frac{1}{Re}\frac{du}{dy} \, dA - \int_{As} \frac{1}{Re}\frac{du}{dy} \, dA - \int_{CV} \frac{dP}{dx} dV \\ + \int_{CV} S_u \, dV\end{aligned}$$

$$\begin{aligned}\int_{Ae} \vec{u}v \, dA - \int_{Aw} \vec{u}v \, dA + \int_{An} \vec{v}v \, dA - \int_{As} \vec{v}v \, dA \\ = \int_{Ae} \frac{1}{Re}\frac{dv}{dx} \, dA - \int_{Aw} \frac{1}{Re}\frac{dv}{dx} \, dA \\ + \int_{An} \frac{1}{Re}\frac{dv}{dy} \, dA - \int_{As} \frac{1}{Re}\frac{dv}{dy} \, dA - \int_{CV} \frac{dP}{dy} dV \\ + \int_{CV} S_u \, dV\end{aligned}$$

$$\int_{Ae} udA - \int_{Aw} udA + \int_{An} vdA - \int_{An} vdA = 0$$

This evaluates to:

$$\begin{aligned}\mathrm{A_e}(\vec{u}u)|_e - \mathrm{A_w}(\vec{u}u)|_w + \mathrm{A_n}(\vec{v}u)|_n - \mathrm{A_s}(\vec{v}u)|_s \\ = \frac{1}{Re}\mathrm{A_e}\left.\frac{du}{dx}\right|_e - \frac{1}{Re}\mathrm{A_w}\left.\frac{du}{dx}\right|_w + \frac{1}{Re}\mathrm{A_n}\left.\frac{du}{dy}\right|_n \\ - \frac{1}{Re}\mathrm{A_s}\left.\frac{du}{dy}\right|_s - \frac{dP}{dx}\Delta V + S_u \Delta V\end{aligned}$$

$$\begin{aligned}\mathrm{A_e}(\vec{u}v)|_e - \mathrm{A_w}(\vec{u}v)|_w + \mathrm{A_n}(\vec{v}v)|_n - \mathrm{A_s}(\vec{v}v)|_s \\ = \frac{1}{Re}\mathrm{A_e}\left.\frac{dv}{dx}\right|_e - \frac{1}{Re}\mathrm{A_w}\left.\frac{dv}{dx}\right|_w + \frac{1}{Re}\mathrm{A_n}\left.\frac{dv}{dy}\right|_n \\ - \frac{1}{Re}\mathrm{A_s}\left.\frac{dv}{dy}\right|_s - \frac{dP}{dy}\Delta V + S_u \Delta V\end{aligned}$$

$$\mathrm{A_e}(\vec{u})|_e - \mathrm{A_w}(\vec{u})|_w + \mathrm{A_n}(\vec{v})|_n - \mathrm{A_s}(\vec{v})|_s = 0$$

2.2 Differencing Scheme

Using central the differencing technique, u is differentiated as follows (v is analogous):

$$\left.\frac{du}{dx}\right|_e = \frac{u_e - u_p}{dx_{ep}} \;\&\; \left.\frac{du}{dx}\right|_w = \frac{u_p - u_w}{dx_{pw}} \;\&\; \left.\frac{du}{dy}\right|_n = \frac{u_n - u_p}{dy_{np}} \;\&\; \left.\frac{du}{dy}\right|_s = \frac{u_p - u_s}{dy_{ps}}$$

This yields (v is analogous):

$$\begin{aligned}\mathrm{A_e}(\vec{u}u)|_e - \mathrm{A_w}(\vec{u}u)|_w + \mathrm{A_n}(\vec{v}u)|_n - \mathrm{A_s}(\vec{v}u)|_s \\ = \frac{1}{Re}\mathrm{A_e}\frac{u_e - u_p}{dx_{ep}} - \frac{1}{Re}\mathrm{A_w}\frac{u_p - u_w}{dx_{pw}} \\ + \frac{1}{Re}\mathrm{A_n}\frac{u_n - u_p}{dy_{np}} - \frac{1}{Re}\mathrm{A_s}\frac{u_p - u_s}{dy_{ps}} - \frac{dP}{dx}\Delta V \\ + S_u \Delta V\end{aligned}$$

From this the following coefficients are defined to simplify the equations (F_e and D_e are shown the rest are analogous):

$$D_e = \frac{\mathrm{A_e}}{Re \cdot dx_{ep}} = \frac{dy_p}{Re \cdot dx_{ep}}$$

$$\mathrm{F}_e = (\mathrm{A}u)_\mathrm{e} = (u)_e dy_p = \left\{ \frac{u_E + u_P}{2} + \frac{1}{2}\left[\frac{dy_E}{a_{PE}}(P_{ee} - P_e) + \frac{dy_P}{a_{PP}}(P_e - P_w)\right] - \frac{dy_E}{\left(\frac{a_{PE}+a_{PP}}{2}\right)}(P_E - P_P)\right\} dy_p$$

$$= \left\{ \frac{u_E + u_P}{2} + \frac{1}{2}\left[\frac{dy_E}{a_{PE}}\left(\frac{P_{EE} - P_P}{2}\right) + \frac{dy_P}{a_{PP}}\left(\frac{P_E - P_W}{2}\right)\right] - \frac{dy_E}{\left(\frac{a_{PE}+a_{PP}}{2}\right)}(P_E - P_P)\right\} dy_p$$

This yields:

$$\mathrm{F}_e u_e - \mathrm{F}_w u_w + \mathrm{F}_n u_n - \mathrm{F}_s u_s = D_e(u_e - u_p) - D_w(u_p - u_w) + D_n(u_n - u_p) - D_s(u_p - u_s) - (P_e - P_w)dy_p$$

Control volume contributions for both non-uniform and uniform grids are defined by η_e, η_w, η_n and η_s. Face velocity equalities are in the following form for central differencing:

$$u_e = \eta_e u_e + (1 - \eta_e)u_p$$

Rearranging the equation to isolate the coefficients for u_p, u_e, u_w, u_n, u_s yields:

$$[(D_e - \mathrm{F}_e\eta_e) + (D_w + \mathrm{F}_w\eta_w) + (D_n - \mathrm{F}_n\eta_n) + (D_s + \mathrm{F}_s\eta_s) + \mathrm{F}_e - \mathrm{F}_w + \mathrm{F}_n - \mathrm{F}_s]u_p = (D_e - \mathrm{F}_e\eta_e)u_e + (D_w + \mathrm{F}_w\eta_w)u_w + (D_n - \mathrm{F}_n\eta_n)u_n + (D_s - \mathrm{F}_s\eta_s)u_s - (\eta_e P_e - \eta_w P_w)dy_p$$

The general coefficients for central differencing are summarized in the following table [1]:

a_p	$(D_e - \mathrm{F}_e\eta_e) + (D_w + \mathrm{F}_w\eta_w) + (D_n - \mathrm{F}_n\eta_n) + (D_s + \mathrm{F}_s\eta_s) + \mathrm{F}_e - \mathrm{F}_w + \mathrm{F}_n - \mathrm{F}_s$
a_e	$(D_e - \mathrm{F}_e\eta_e)$
a_w	$(D_w + \mathrm{F}_w\eta_w)$
a_n	$(D_n - \mathrm{F}_n\eta_n)$
a_s	$(D_s - \mathrm{F}_s\eta_s)$

2.3 Upwind Scheme

For Upwind Differencing the following equalities are assumed if u > 0 (assuming the definition of the standard coordinate system):

$$u_e = u_p \;\&\; u_w = u_w \;\&\; u_n = u_p \;\&\; u_s = u_s$$

Rearranging the equation to isolate the coefficients for u_p, u_e, u_w, u_n, u_s yields:

$$[(D_e) + (D_w + \mathrm{F}_w) + (D_n) + (D_s + \mathrm{F}_s) + \mathrm{F}_e - \mathrm{F}_w + \mathrm{F}_n - \mathrm{F}_s]u_p = (D_e)u_e + (D_w + \mathrm{F}_w)u_w + (D_n)u_n + (D_s + \mathrm{F}_s)u_s - \left(\left[\eta_e P_e + (1 - \eta_e)P_p\right] - \left[\eta_w P_w + (1 - \eta_w)P_p\right]\right)dy_p$$

For Upwind Differencing the following equalities are assumed if u < 0 (assuming the definition of the standard coordinate system):

$$u_e = u_e \;\&\; u_w = u_p \;\&\; u_n = u_n \;\&\; u_s = u_p$$

Rearranging the equation to isolate the coefficients for u_p, u_e, u_w, u_n, u_s yields:

$$[(D_e - \mathrm{F}_e) + (D_w) + (D_n - \mathrm{F}_n) + (D_s) + \mathrm{F}_e - \mathrm{F}_w + \mathrm{F}_n - \mathrm{F}_s]u_p = (D_e - \mathrm{F}_e)u_e + (D_w)u_w + (D_n - \mathrm{F}_n)u_n + (D_s)u_s - \left(\left[\eta_e P_e + (1 - \eta_e)P_p\right] - \left[\eta_w P_w + (1 - \eta_w)P_p\right]\right)dy_p$$

The upwind equations for each case can be combined into the following equation:

$$\left[\left(D_e + \max(0, -\mathrm{F}_e)\right) + \left(D_w + \max(0, \mathrm{F}_w)\right) + \left(D_n + \max(0, -\mathrm{F}_n)\right) + \left(D_s + \max(0, \mathrm{F}_s)\right) + \mathrm{F}_e - \mathrm{F}_w + \mathrm{F}_n - \mathrm{F}_s\right]u_p = \left(D_e + \max(0, -\mathrm{F}_e)\right)u_e + \left(D_w + \max(0, \mathrm{F}_w)\right)u_w + \left(D_n + \max(0, -\mathrm{F}_n)\right)u_n + \left(D_s + \max(0, \mathrm{F}_s)\right)u_s$$

The general coefficients for the upwind method are summarized in the following table [1]:

a_p	$\left(D_e + \max(0, -F_e)\right) + \left(D_w + \max(0, F_w)\right) + \left(D_n + \max(0, -F_n)\right) + \left(D_s + \max(0, F_s)\right) + F_e - F_w + F_n - F_s$
a_e	$\left(D_e + \max(0, -F_e)\right)$
a_w	$\left(D_w + \max(0, F_w)\right)$
a_n	$\left(D_n + \max(0, -F_n)\right)$
a_s	$\left(D_s + \max(0, F_s)\right)$

2.4 Continuity Pressure Correction

The continuity equation will be used for pressure correction:

$$F_e - F_w + F_n - F_s = 0$$

$$(u)_e dy_p - (u)_w dy_p + (v)_n dx_p - (v)_s dx_p = 0$$

$$\left[u_e^* + \frac{A_e}{a_{pe}}\left(P_p' - P_e'\right)\right] dy_p - \left[u_w^* + \frac{A_w}{a_{pw}}\left(P_w' - P_p'\right)\right] dy_p + \left[v_n^* + \frac{A_n}{ap_n}\left(P_p' - P_n'\right)\right] dx_p - \left[v_s^* + \frac{A_s}{a_{ps}}\left(P_s' - P_p'\right)\right] dx_p = 0$$

$$\frac{A_e}{a_{pe}} dy_p P_p' - \frac{A_e}{a_{pe}} dy_p P_e' - \frac{A_w}{a_{pw}} dy_p P_w' + \frac{A_w}{a_{pw}} dy_p P_p' + \frac{A_n}{a_{pn}} dx_p P_p' - \frac{A_n}{a_{pn}} dx_p P_n' - \frac{A_s}{a_{ps}} dx_p P_s' + \frac{A_s}{a_{ps}} dx_p P_p' = (u_w^* - u_e^*) dy_p + (v_s^* - v_n^*) dx_p$$

$$\left(\frac{A_e}{a_{pe}} dy_p + \frac{A_w}{a_{pw}} dy_p + \frac{A_n}{a_{pn}} dx_p + \frac{A_s}{a_{ps}} dx_p\right) P_p' = \left(\frac{A_e}{a_{pe}} dy_p\right) P_e' + \left(\frac{A_w}{a_{pw}} dy_p\right) P_w' + \left(\frac{A_n}{a_{pn}} dx_p\right) P_n' + \left(\frac{A_s}{a_{ps}} dx_p\right) P_s' + (u_w^* - u_e^*) dy_p + (v_s^* - v_n^*) dx_p$$

$$\left(\frac{{dy_p}^2}{a_{pe}} + \frac{{dy_p}^2}{a_{pw}} + \frac{{dx_p}^2}{a_{pn}} + \frac{{dx_p}^2}{a_{ps}}\right) P_p' = \left(\frac{{dy_p}^2}{a_{pe}}\right) P_e' + \left(\frac{{dy_p}^2}{a_{pw}}\right) P_w' + \left(\frac{{dx_p}^2}{a_{pn}}\right) P_n' + \left(\frac{{dx_p}^2}{a_{ps}}\right) P_s' + (u_w^* - u_e^*) dy_p + (v_s^* - v_n^*) dx_p$$

Where the following coefficients are the averages of the a_p coefficients in the momentum equations, for example:

$$a_{pe} = \frac{1}{2}(a_{PE} + a_{PP})$$

The following velocities are used for the source term. The velocity equations are modified using the term after the "&" in place of the other pressure average terms where appropriate in locations at or near the boundary. Note these face velocity equations are also used to update F coefficient values as shown above.

$$u_e = \frac{u_E + u_P}{2} + \frac{1}{2}\left[\frac{dy_E}{a_{PE}}\left(\frac{P_{EE} - P_P}{2}\right) + \frac{dy_P}{a_{PP}}\left(\frac{P_E - P_W}{2}\right)\right] - \frac{dy_E}{\left(\frac{a_{PE} + a_{PP}}{2}\right)}(P_E - P_P) \& \left(\frac{P_E - P_P}{2}\right)$$

$$u_w = \frac{u_W + u_P}{2} + \frac{1}{2}\left[\frac{dy_E}{a_{PW}}\left(\frac{P_P - P_{WW}}{2}\right) + \frac{dy_P}{a_{PP}}\left(\frac{P_E - P_W}{2}\right)\right] - \frac{dy_W}{\left(\frac{a_{PW} + a_{PP}}{2}\right)}(P_P - P_W) \& \left(\frac{P_P - P_W}{2}\right)$$

$$v_n = \frac{v_N + v_P}{2} + \frac{1}{2}\left[\frac{dx_N}{a_{PN}}\left(\frac{P_{NN} - P_P}{2}\right) + \frac{dx_P}{a_{PP}}\left(\frac{P_N - P_S}{2}\right)\right] - \frac{dx_N}{\left(\frac{a_{PN} + a_{PP}}{2}\right)}(P_N - P_P) \& \left(\frac{P_N - P_P}{2}\right)$$

$$v_s = \frac{v_S + v_P}{2} + \frac{1}{2}\left[\frac{dx_S}{a_{PS}}\left(\frac{P_P - P_{SS}}{2}\right) + \frac{dx_P}{a_{PP}}\left(\frac{P_N - P_S}{2}\right)\right] - \frac{dx_S}{\left(\frac{a_{PS} + a_{PP}}{2}\right)}(P_P - P_S) \& \left(\frac{P_P - P_S}{2}\right)$$

The general coefficients for the pressure correction are summarized in the following table:

P_p'	$\left(\frac{{dy_p}^2}{a_{pe}} + \frac{{dy_p}^2}{a_{pw}} + \frac{{dx_p}^2}{a_{pn}} + \frac{{dx_p}^2}{a_{ps}}\right)$
P_e'	$\left(\frac{{dy_p}^2}{a_{pe}}\right)$
P_w'	$\left(\frac{{dy_p}^2}{a_{pw}}\right)$

P_n'	$\left(\frac{dx_p{}^2}{a_{pn}}\right)$
P_s'	$\left(\frac{dx_p{}^2}{a_{ps}}\right)$

2.5 Velocity and Pressure Corrections

Values for u, v and p are corrected using the following formulas:

$$u = u^* + \frac{A}{a_p}(P_w' - P_e') = u^* + \frac{dy_p}{a_{PP}}(P_w' - P_e')$$

$$v = v^* + \frac{A}{a_p}(P_w' - P_e') = v^* + \frac{dx_p}{a_{PP}}(P_s' - P_n')$$

$$P = P^* + P'$$

Values for F_e, F_w, F_n, F_s are corrected using the following formulas:

$$\mathrm{F}_e = \mathrm{F}_e + \frac{A_e}{a_{pe}}(P_p' - P_e')dy_p = \mathrm{F}_e + \frac{dy_p{}^2}{\frac{1}{2}(a_{PE} + a_{PP})}(P_p' - P_e')$$

$$\mathrm{F}_w = \mathrm{F}_w + \frac{A_w}{a_{pw}}(P_w' - P_p')dy_p = \mathrm{F}_w + \frac{dy_p{}^2}{\frac{1}{2}(a_{PW} + a_{PP})}(P_w' - P_p')$$

$$\mathrm{F}_n = \mathrm{F}_n + \frac{A_n}{a_{pn}}(P_p' - P_n')dx_p = \mathrm{F}_n + \frac{dx_p{}^2}{\frac{1}{2}(a_{PN} + a_{PP})}(P_p' - P_n')$$

$$\mathrm{F}_s = \mathrm{F}_s + \frac{A_s}{a_{ps}}(P_s' - P_p')dx_p = \mathrm{F}_s + \frac{dx_p{}^2}{\frac{1}{2}(a_{PS} + a_{PP})}(P_s' - P_p')$$

3.0 Numerical Implementation

3.1 General Program Structure

The code has been broken up into several subroutines. The main program simply calls each of the major subroutines in sequence to solve the problem. Before the subroutines are called, a module allows allocatable arrays to be passed into subroutines as arguments as they are needed. The first subroutine reads in a user input file and stores all of the problem parameters as variables for use by other subroutines. The second subroutine uses the parameters in the input file to generate initial velocity and pressure values and to generate all problem geometry including: both uniform and non-uniform mesh geometry, coordinate locations for each control volume center, distances between control volume centers (i.e. dx_{wp}, dx_{pe}) and distances across control volume faces (dx_p, dy_p). These are shown in Figure 2 Discrete Control Volume Geometry.

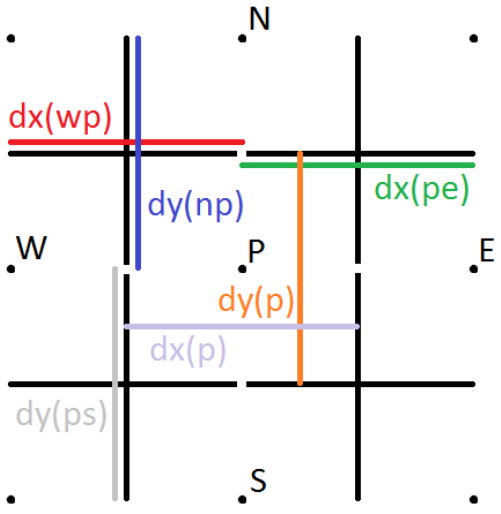

Figure 2 Discrete Control Volume Geometry

The third subroutine is the main solver, it calls and interacts with several other subroutines. It works alongside the face velocity solver subroutine, the tridiagonal matrix algorithm subroutine, the central difference and upwind scheme subroutines, and finally sends outputs to the output file subroutine. In addition to interacting with these subroutines this subroutine sets boundary conditions for the problem, initializes final velocity and pressure values, calculates F and D coefficients, solves the velocity momentum equations, the pressure correction equation, corrects velocities and pressures and iterates the entire process until convergence. This solver is described in more detail in 3.2 Main Solver.

The face velocity solver determines the face velocities across each control volume in the x and y directions. There are special cases for each corner control volume, each border, each row and column one inside the border and each inner corner connecting these inner rows and columns. The face velocity equations described in 2.4 Continuity Pressure Correction are used. These equations are modified for each of the cases mentioned above. The modification is either applying a boundary velocity, setting the face velocity to 0 in cases where the face exists outside the domain, applying the velocity equation as is, or applying the velocity equation modified by the term at the end replacing the pressure difference term that would result in an out of bounds array error.

A solution method subroutine chooses between the upwind scheme subroutine and the central difference subroutine. These subroutines then generate the coefficients used to solve the momentum equations and the pressure correction equation.

Once a converged solution is obtained the results are sent to the final subroutine which outputs the results in a formatted

text file useable by MATLAB and Excel and also outputs a formatted data file for Tecplot.

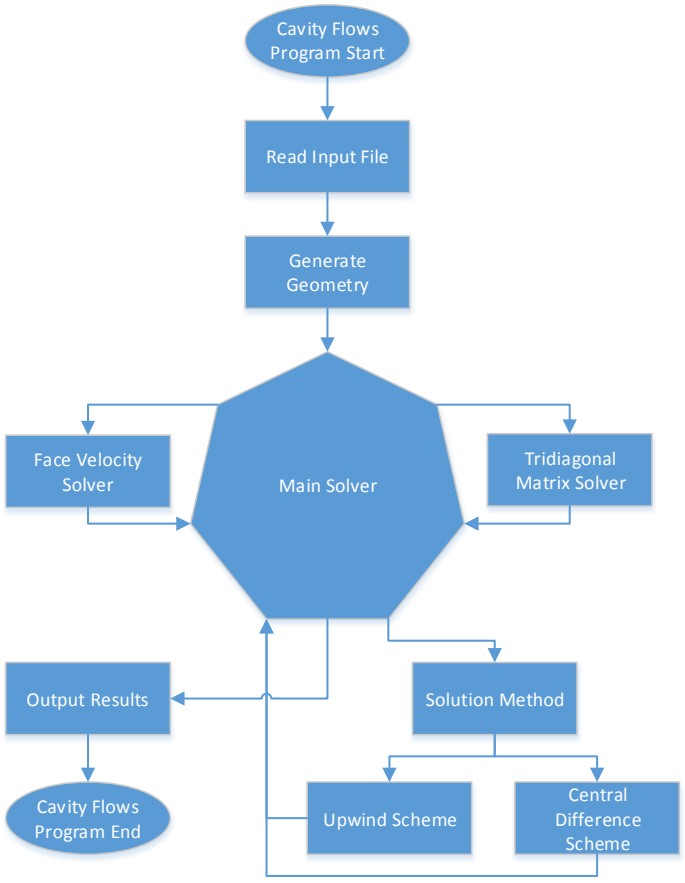

Figure 3 Program Flowchart

3.2 Main Solver

The main solver uses the collocated SIMPLE algorithm to find a converged solution. Before the algorithm starts, final arrays are populated with boundary velocities and guesses for pressure, pressure correction and a_p coefficients.

The first step is to calculate face velocities at each control volume face for each control volume in the domain. This is performed as described in 3.1 General Program Structure. The equations used to calculate face velocities include pressure, velocity and a_p coefficients which for this first pass are provided as guesses (except for boundary condition velocities). These face velocities will then be used to calculate F coefficients for convective flux. D coefficients for diffusion are also calculated at this point. Since face velocities will change over the course of the solution process, the convective flux coefficients will periodically be recalculated.

The second step is to solve the momentum equations for velocity in the x and y directions until convergence. This is the first procedure in the major iteration loop. Before this can occur however a_p, a_e, a_w, a_n, a_s coefficients are calculated according to either the upwind or central difference scheme. Then the pressure source terms in the momentum equations are calculated. From here a relaxation factor is applied to both the a_p coefficient and the pressure source terms. This works to affect each of the momentum and pressure correction equations all at once [2]. Since the momentum solver implementation solves for the entire domain, the boundary conditions need to be re-established at this point. Once they've been established they need to be fixed by adding a number of large magnitude to the a_p coefficients and to the right side of the equation. At this point the solvers for velocity in the x and y direction can be entered. In these solvers several linear arrays are populated with a coefficients and source terms. These arrays form the inputs used to solve for velocities by the TDMA. This is performed iteratively from left to right, column by column and iterated until converged values are obtained. This is performed separately for both the x momentum and the y momentum.

The third step is to update the face velocities using the converged x and y velocities and then use these updated velocities to calculate F coefficients used in the pressure correction equation. In this step the face velocity solver described in 3.1 General Program Structure is called and then F convective flux coefficients are recalculated.

The fourth step is to solve for a converged value of pressure correction. The coefficients used to solve for pressure correction are in 2.4 Continuity Pressure Correction. These equations use 'a' coefficients and are calculated for each pressure coefficient for each control volume including those at the boundaries. Once the coefficients are found they are used in solving pressure corrections in the same manner that velocities were solved.

The fifth step is to correct the velocities and pressure using the converged values of pressure correction as well as to correct the F coefficients using pressure correction. The equations for this are in 2.5 Velocity and Pressure Corrections.

The final step is to repeat the process from step two until a converged solution is obtained. This converged solution occurs when the value of $\sum \dot{m}$ stops getting smaller as it approaches 0.

The box is applied by first determining which node the box ends at along the x and y axis. Once this is determined the velocity values in the region of the box are initialized to 0 just before the momentum solvers are entered. Also the a_p coefficients along with the ride side of the equation have a number of large magnitude added to them in order to fix the velocities for these points.

4.0 Results and Discussion

4.1 Reynolds Number Comparison

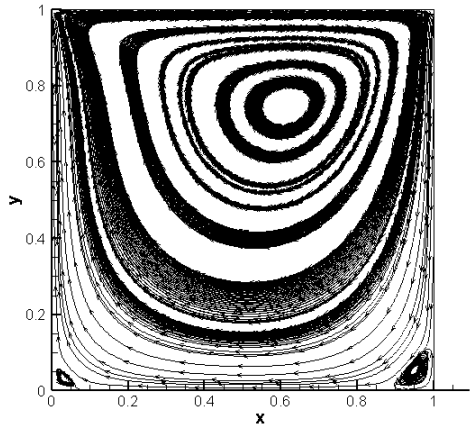

60x60, 100Re, Uniform, Upwind

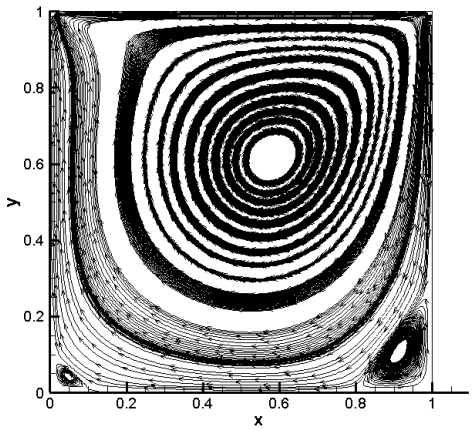

60x60, 400Re, Uniform, Upwind

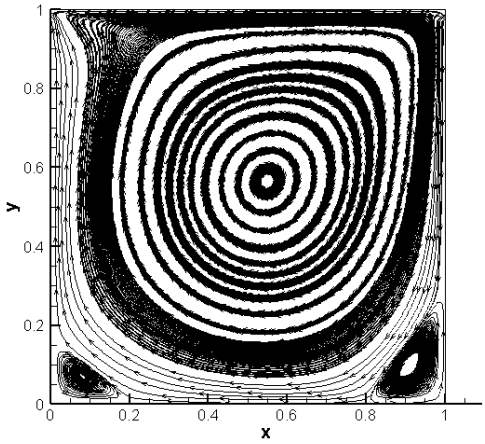

60x60, 1000Re, Uniform, Upwind

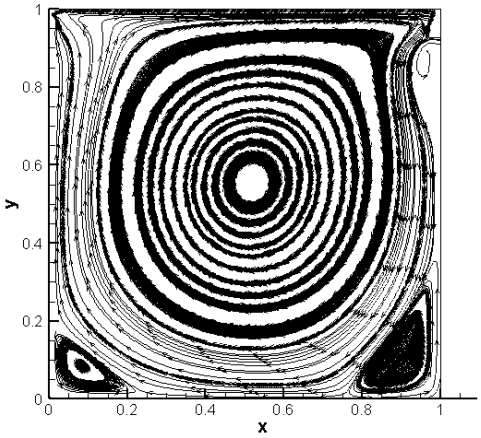

60x60, 3200Re, Uniform, Upwind

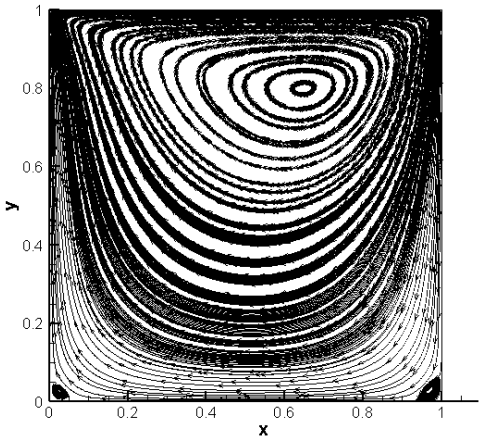

120x120, 100Re, Uniform, Upwind

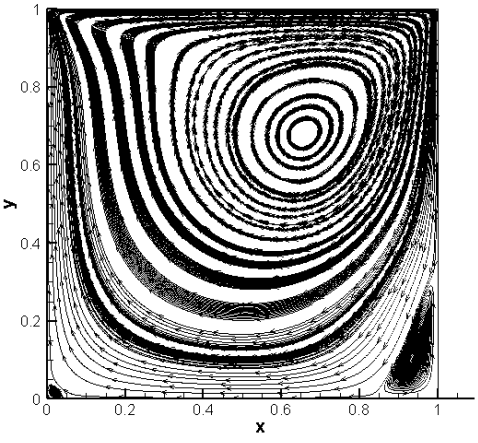

120x120, 400Re, Uniform, Upwind

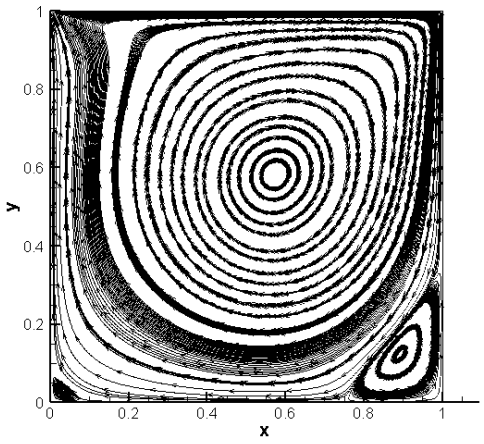

120x120, 1000Re, Uniform, Upwind

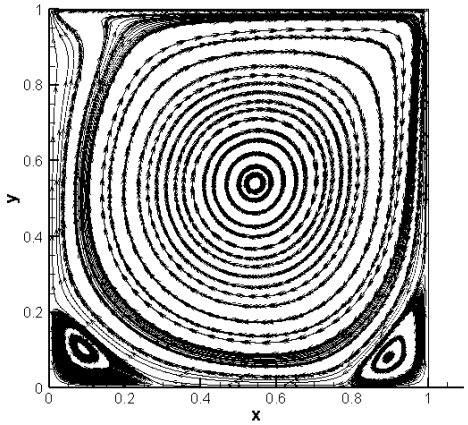

120x120, 3200Re, Uniform, Upwind

A no slip boundary condition exists in which the velocity of the flow at the boundaries equals the velocity of the boundary, this means that there is 0 velocity at the stationary boundaries and a velocity equal to the lid velocity along the top boundary. The flow in the rest of the domain is driven by pressure and frictional shear forces. The dimensionless discretization of the collocated SIMPLE algorithm allows all the information for the flow behaviour (outside of boundary conditions) to be determined by the Reynolds number. The Reynolds number (Re) relates each of the density, velocity, characteristic length and viscosity variables into a single dimensionless quantity.

Results were generated at different Re for two mesh resolutions: 60x60 and 120x120. In general for both mesh resolutions increasing the Re moves the center of rotation of the velocity field from the top right at low Re to the very center at high Re. Increasing the Re also causes the vortices in the corners to become larger and more prominent. At the highest tested Re of 3200 the vortex at the bottom left corner approaches the size as the vortex in the bottom right. Also notable is the behaviour of the top corners for the high Re of 3200. For the mesh size of 60x60 an unexpected vortex appears to begin forming in the top right, however as the mesh size is increased for the same Re this vortex disappears and the expected vortex at the top left corner of the domain begins to form. This agrees with the results found in Ghia et al [3].

These results reinforce the preference towards using a larger mesh size when possible to achieve more accurate results. The results also show that increasing Re causes more and larger vortices to appear and the center of rotation for the velocity field to tend towards the geometric center of the domain. 3200 was the highest Re that the simulation was run at due to processing capability and time constraints. In order to achieve accurate results at Re of 5000 the mesh resolution would also need to be increased to 250x250. When this was attempted it took too long to converge to an accurate solution using the implementation described above and the available resources as far as time and computational capacity.

4.2 Mesh Resolution Comparison

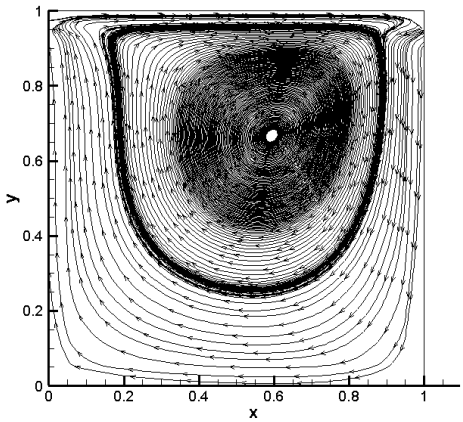

20x20, 400Re, Uniform, Upwind

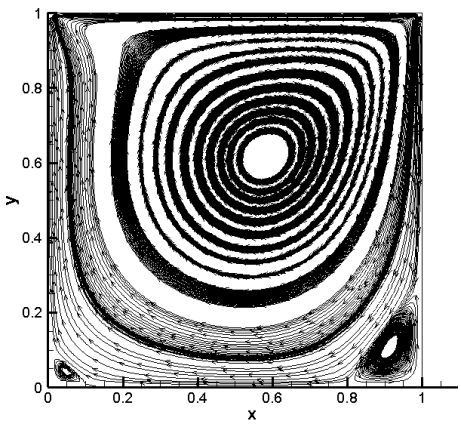

60x60, 400Re, Uniform, Upwind

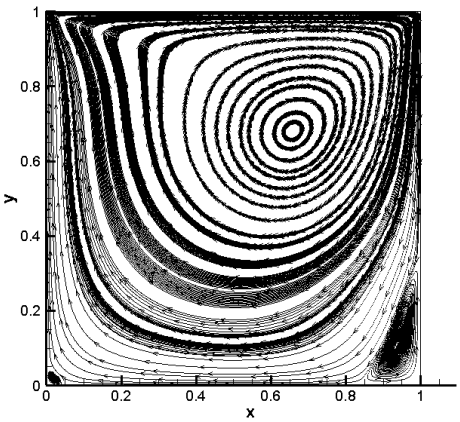

120x120, 400Re, Uniform, Upwind

The results for different mesh resolutions at a Reynolds number (Re) of 400 show that at the smallest mesh size of 20x20 no vortices appear and the velocity field's behaviour at the corners is not well defined. At a mesh size of 60x60 vortices at the corners are visible and the flow at the corners is better defined. For a mesh size of 120x120 the vortices are more accurately proportioned and positioned, also the behaviour at the corners and in the domain is better defined due to the higher resolution and an increase in number of streamlines. This agrees with the results in Ghia et al. [3]. From these results it can be concluded that increasing mesh resolution increases the accuracy of the results.

4.3 Mesh Uniformity Comparison

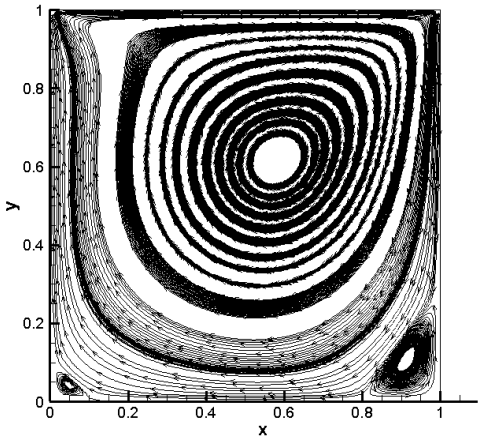

60x60, Uniform, 400Re, Upwind

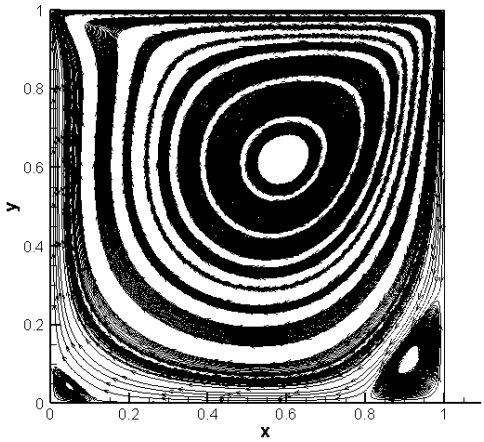

60x60, Non-Uniform (5%), 400Re, Upwind

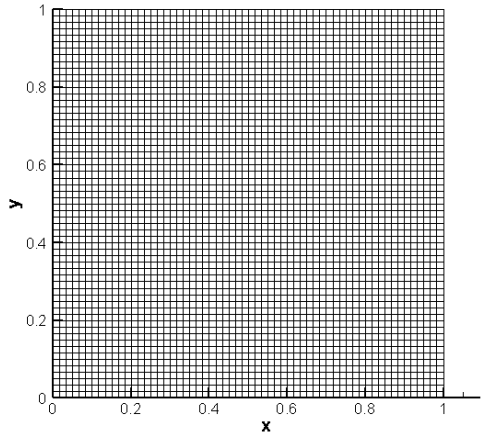

60x60, Uniform Grid

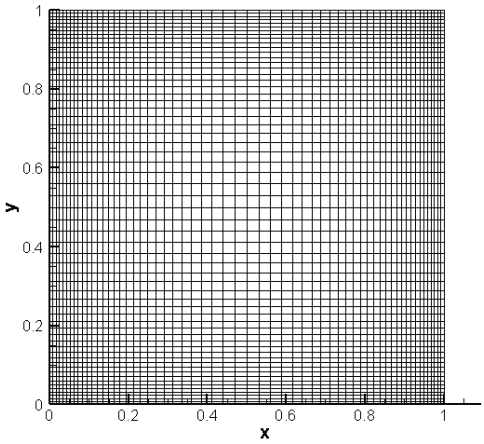

60x60, Non-Uniform Grid (5%)

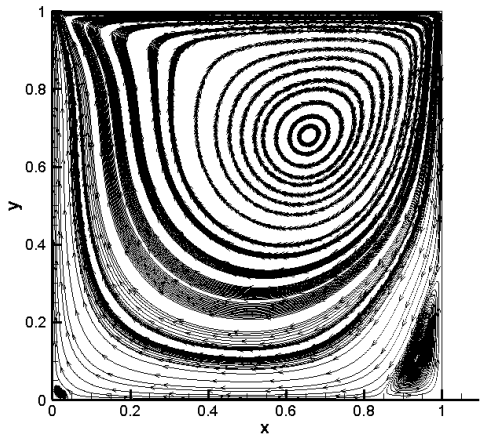

120x120, Uniform, 400Re, Upwind

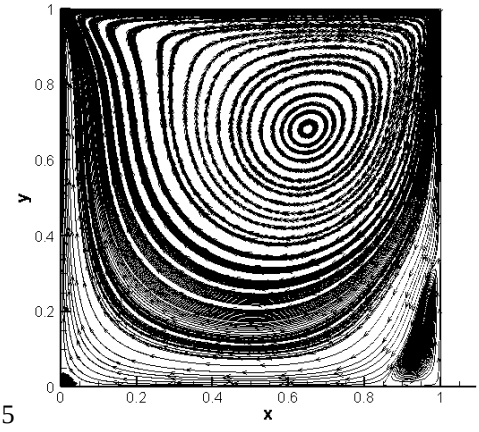

120x120, Non-Uniform (1%), 400Re, Upwind

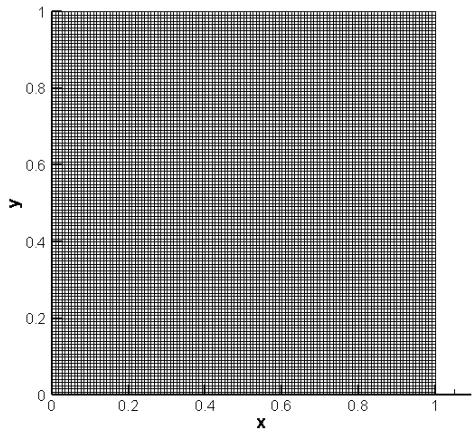

120x120, Uniform Grid

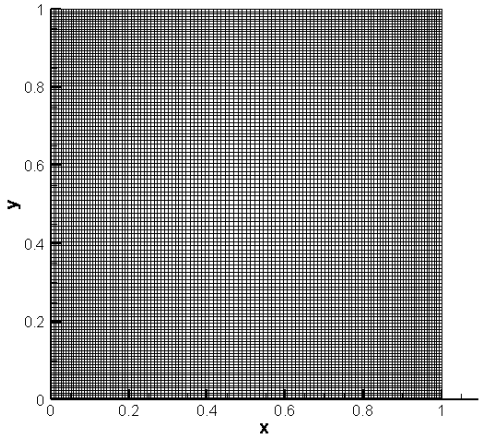

120x120, Non-Uniform Grid (1%)

The results obtained are shown to be generally independent of using a uniform or non-uniform mesh. A mesh resolution of 60x60 and inflation factor of 5% yields comparable results to a uniform mesh. A mesh resolution of 120x120 and inflation factor of 1% also yields comparable results to the uniform mesh. However, it is expected that if very large inflation factors are used then the results would be different and the velocity field would be less accurate near the center and biased towards the areas of small control volume size at the boundaries. From this it can be concluded that using a non-uniform grid will not significantly affect results as long as the inflation factor is not too large and the larger the grid then the smaller the inflation factor needs to be.

4.4 Box Comparison

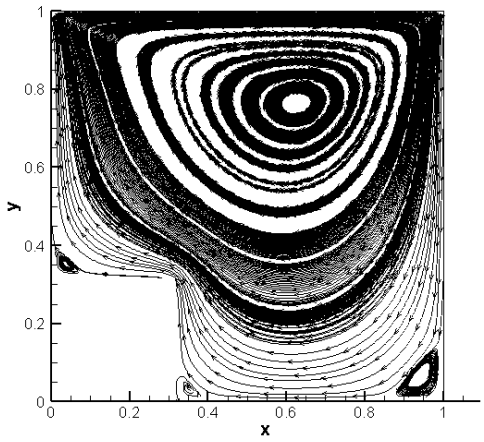

60x60, 100Re, Uniform, Upwind, Box

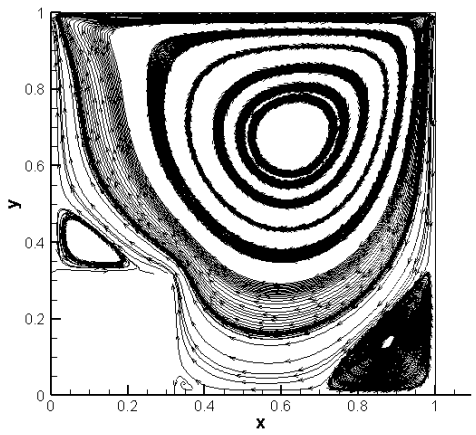

60x60, 400Re, Uniform, Upwind, Box

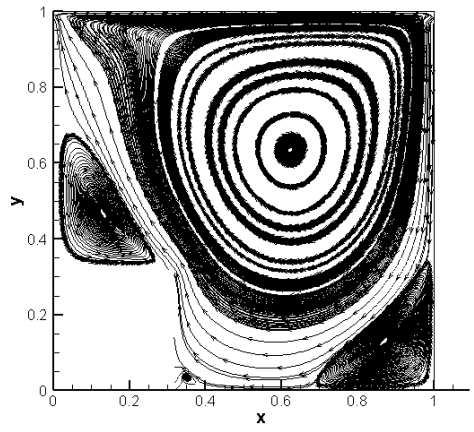

60x60, 1000Re, Uniform, Upwind, Box

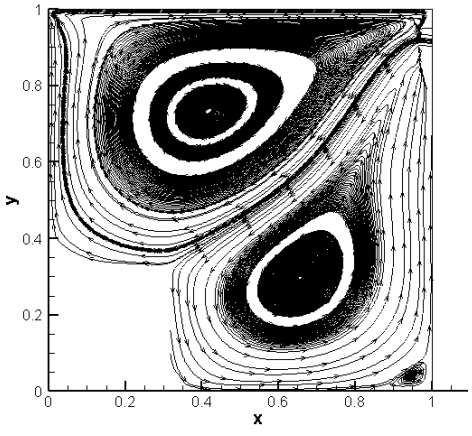

60x60, 3200Re, Uniform, Upwind, Box

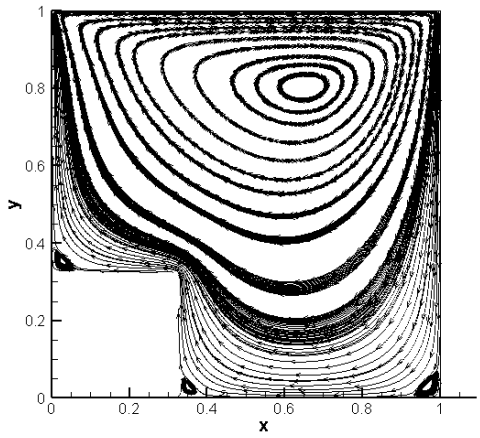

120x120, 100Re, Uniform, Upwind, Box

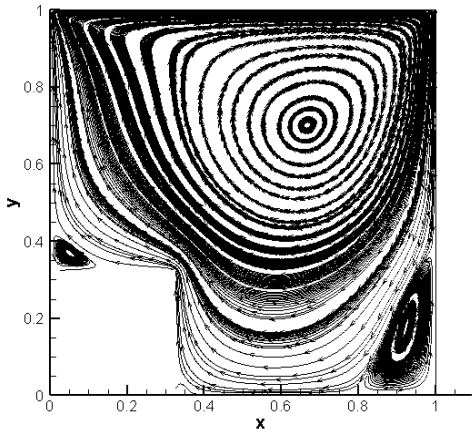

120x120, 400Re, Uniform, Upwind, Box

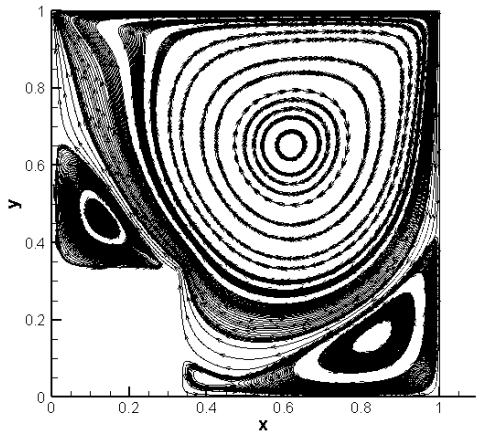

120x120, 1000Re, Uniform, Upwind, Box

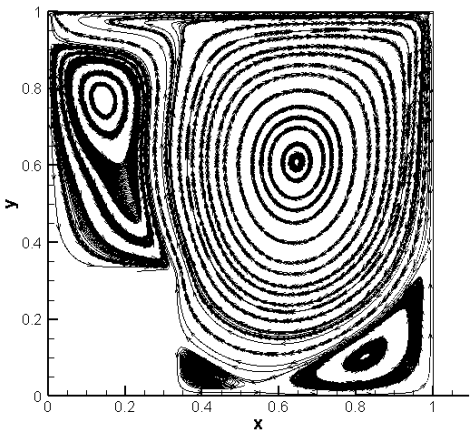

120x120, 3200Re, Uniform, Upwind, Box

Adding a solid box in the corner causes the flow to behave differently around the obstacle. Results were obtained for both a 60x60 mesh resolution and for a 120x120 mesh resolution. Expected results appear for the 60x60 mesh resolution until the Re increases to 3200, at that point the results stop making physical sense. This seems to be a symptom of insufficient mesh resolution. When the mesh resolution is increased to 120x120 expected behaviour occurs for a Re of 3200. In general, the presence of the box causes a large vortex to appear above the box at the domain boundary and a large vortex at the bottom right corner. As the Re increases the vortices along the bottom become large enough to begin merging and the vortex along the left boundary increases in size. These vortices are larger than those created when there is no box.

4.5 Central Difference Comparison

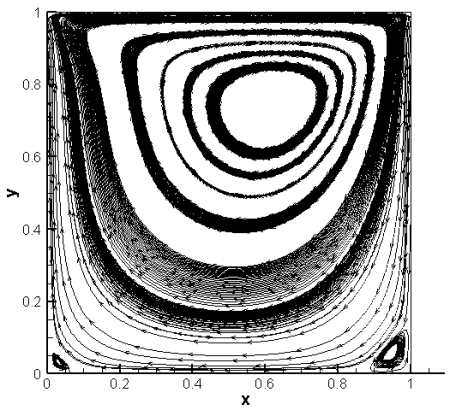

60x60, 100Re, Uniform, Central Difference

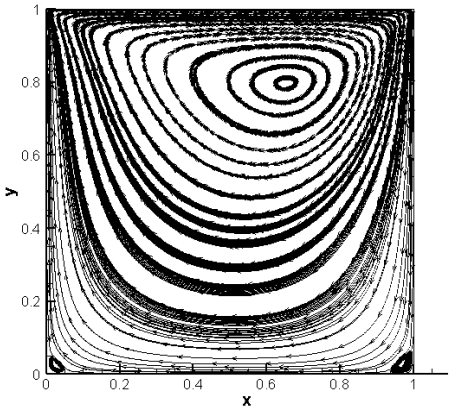

120x120, 100Re, Uniform, Central Difference

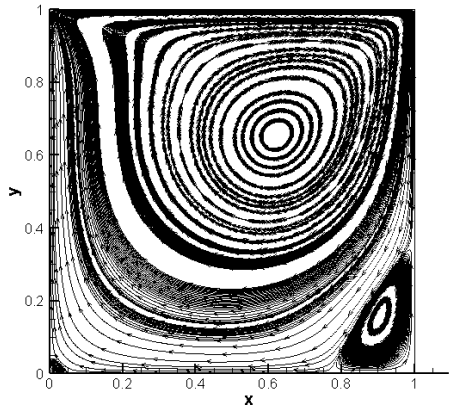

120x120, 400Re, Uniform, Central Difference

The central difference scheme has limitations when compared to the upwind scheme. The central difference scheme requires the Peclet number to be less than 2, where $Pe = \frac{F}{D} = \frac{\vec{u}A}{\frac{A}{\mathrm{Re}dx}} = \vec{u}\mathrm{Re}dx$. Therefore, a relationship can be observed that relates mesh resolution, face velocity and Re with Pe. For a mesh size of 100 it is expected that the central difference scheme will fail at a Re past 200. For a mesh size of 50 it is expected that it will fail at a Re past 100. However the implementation used applies an over relaxation of 0.7 to the a_p term and so a mesh size of 100 using central difference actually fails past a Re of 575 instead of 200 and a mesh size of 50 fails past a Re of 325 instead of 100. As the over relaxation of a_p approaches 1 the central difference scheme will fail at lower Re that approaches 200 for a mesh size of 100 and will fail for a Re approaching 100 for a mesh size of 50. For example, testing the code with a mesh size of 50 and a relaxation of 0.95 results in the scheme failing past a Re of 235. The graphs above show the simulation preformed for several cases using the central difference scheme. The results are the same as for the upwind scheme. In the case of the upwind scheme all Re are expected to work.

4.6 Velocities along Center Axes

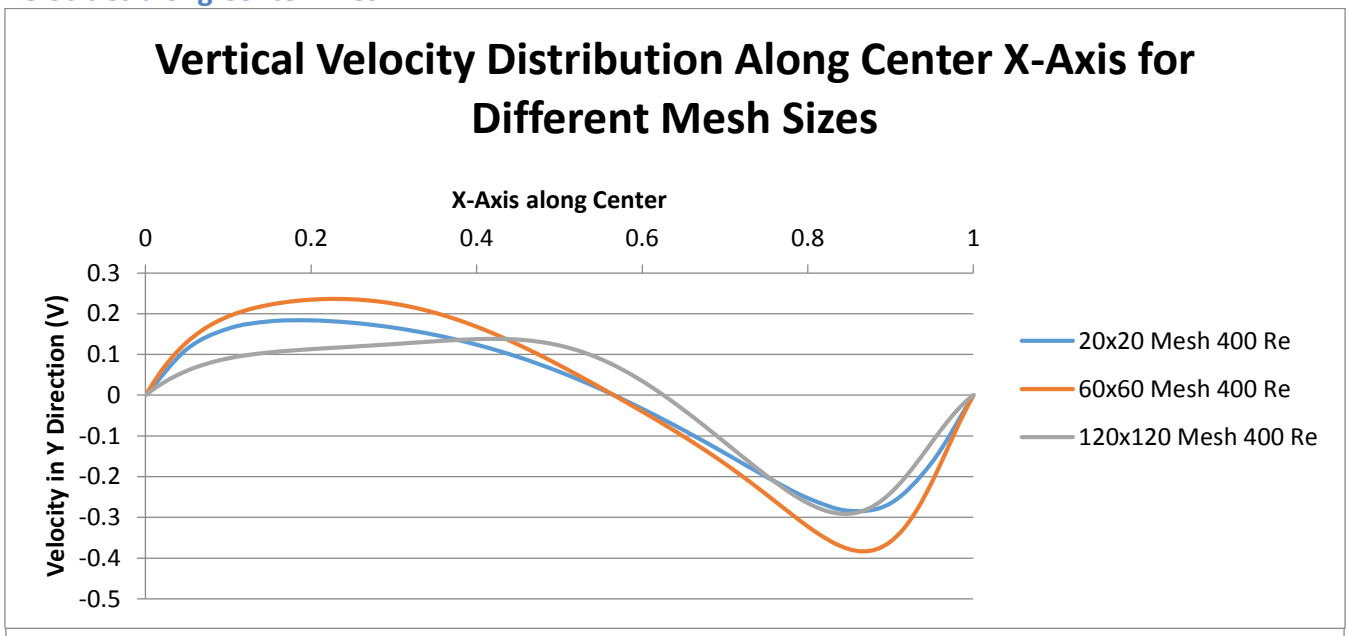

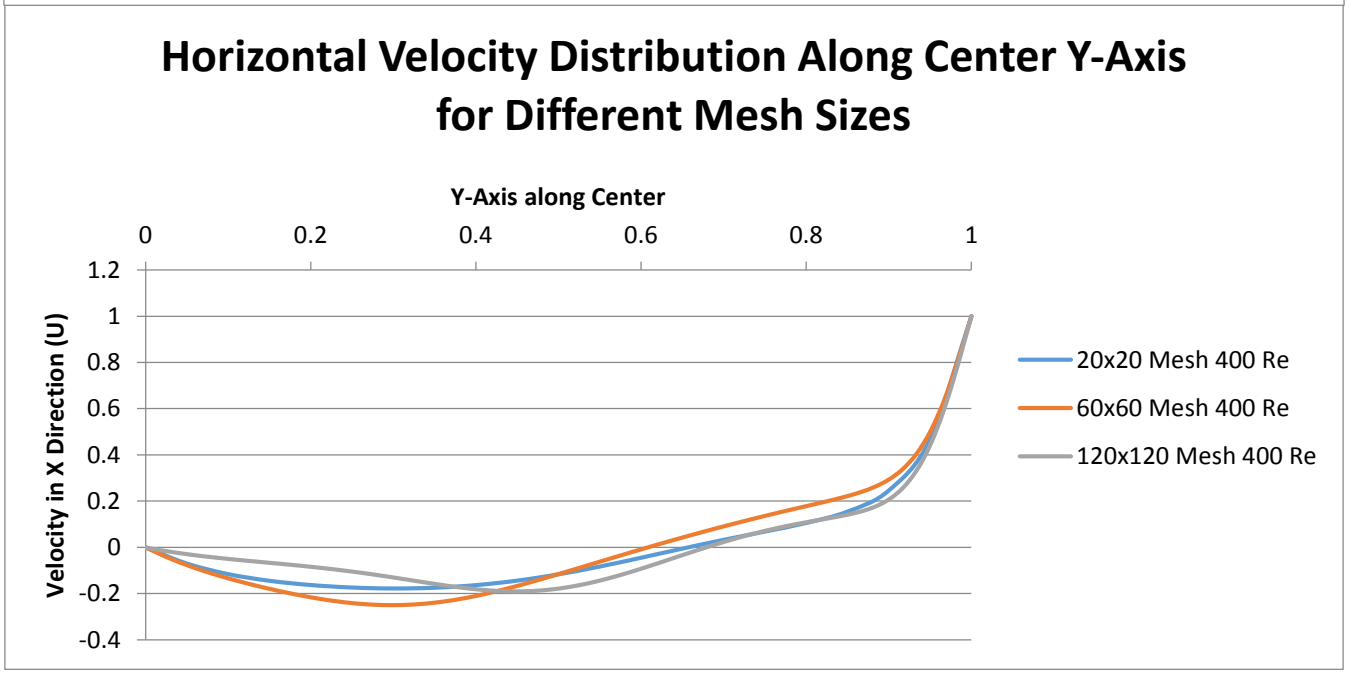

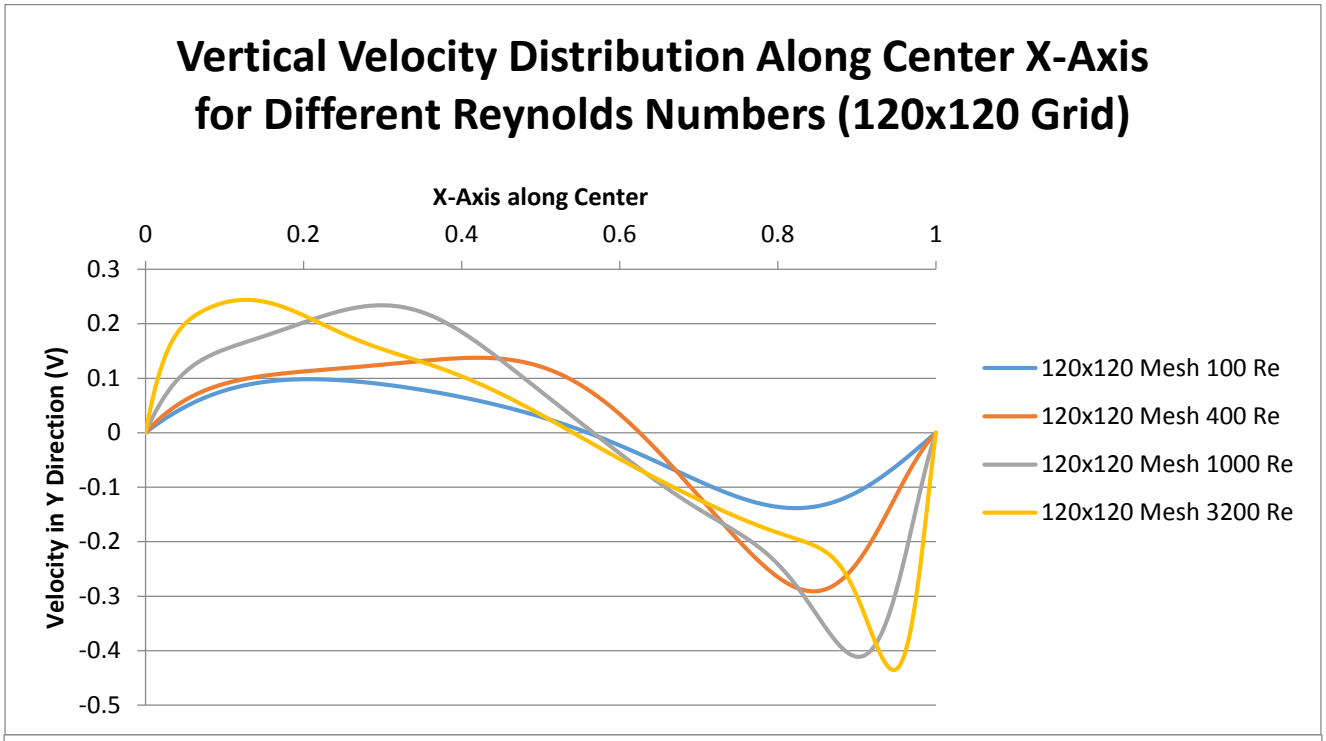

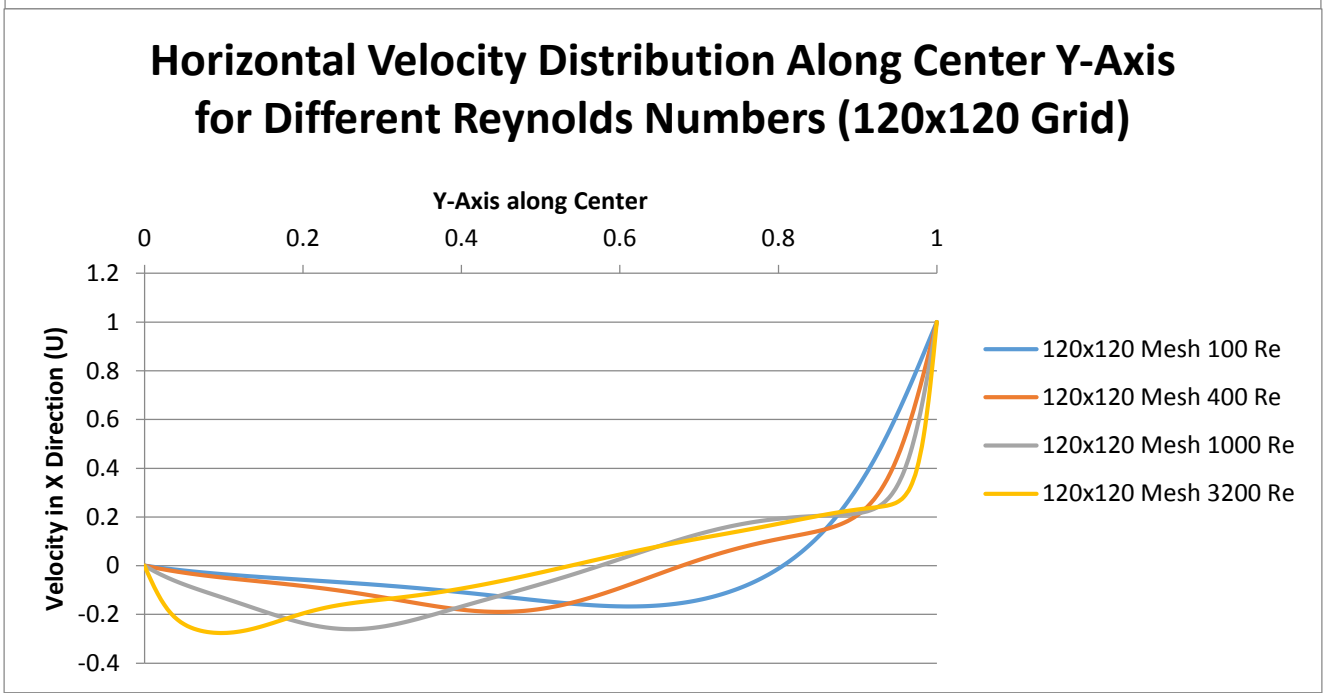

The vertical velocities along the horizontal axis at the center of the domain are positive on the left half as the general direction of the flow is upwards and are negative on the right half with downwards flow. There is no slip at the boundaries so velocity there is 0 on both sides. The main difference between the two sides is the direction that the flow is being driven by the lid causes a greater maximum magnitude for velocity on the right side as the flow has more momentum at that point than it does when it comes around to the right. As far as a quantitative comparison, the curves for different Re at a 120x120 mesh size agree with the results in figure 2b in Ghia et al [3].

In a similar manner, the horizontal velocities along the vertical axis are negative near the bottom half as the flow moves opposite to the direction of the lid and they are positive in the top half as the flow is driven forward by the lid. Due to the no slip condition the

velocity is 0 on the bottom boundary and equal to the lid velocity at the top boundary. The magnitude of the curves for various Re for a mesh size of 120x120 agree with the results in figure 2a in Ghia et al [3].

In both cases, as Re increases the magnitude of the velocities increases and the velocities switch over from positive to negative closer to a value of 0.5 which represents the geometric domain center. Also with an increase in Re the greatest velocities tend towards the boundary while maintaining the no slip condition. Also in both cases as the Re increases to 3200 the velocity profile approaches a linear relationship in the middle of the domain, this indicates uniform vorticity [3]. The plots for a Re of 400 and varying mesh size show that the curve for the highest mesh resolution is the most accurate as it more closely follows the pattern of increasing Re shown in the subsequent graphs.

5.0 Conclusion

Several conclusions can be drawn from the solutions obtained under the various conditions for the lid-driven cavity flow problem. Before running any simulations it was beneficial to non-dimensionalize the Navier-Stokes equation. This allowed all fluid parameters for the problem (aside from boundary conditions) to be represented simply through the Reynolds number.

With regards to the results, gradually increasing Reynolds numbers resulted in the formation of vortices in the bottom two corners of the domain. The vortex formed in the bottom left was larger than the one in the bottom right initially but as Reynolds number increased it the bottom right vortex also increased in size and a vortex began forming in the top left corner of the domain. Also the center of rotation for the vortex in the middle tended towards the geometric center of the control volume with higher Reynolds numbers. At higher Reynolds numbers, larger mesh resolutions were required to ensure accurate results.

The uniformity of the mesh was shown to be independent of the results when the inflation factor was not too large. Smaller mesh sizes are more tolerant of larger inflation factors while larger mesh sizes require smaller inflation factors to maintain accurate results.

When adding a box, a large vortex formed above the box at the domain boundary and a large vortex formed at the bottom right corner. A smaller vortex formed at the bottom left corner of the box and as the Re increased the vortices along the bottom became large enough to begin merging and the vortex along the left boundary increased in size. In these tests the need for a high resolution for high Reynolds numbers was enforced.

When comparing schemes it was found that the central difference scheme was less robust than the upwind scheme. The upwind scheme works for all cases but the central difference scheme theoretically fails when the Reynolds number is twice the mesh resolution. The implementation used allowed the central difference scheme to work beyond this but it still failed at low Reynolds numbers.

Higher mesh resolutions result in greater accuracy but at the cost of increased computational cost. Higher Reynolds number solutions require tighter convergence criteria, greater mesh resolutions and generally need more iterations in order to yield converged, accurate results. Each of these additional requirements also increases computational cost. As a result the highest Reynolds number with a converged result was 3200. Higher numbers were attempted but limitations prevented converged results.

References

[1] W. H.K. Versteeg, An introduction to computational fluid dynamics: The finite volume method, Toronto: Pearson, 2007.

[2] M. Kiričkov, "Solution of the momentum equations for U and V," cfd-online.com, 2010. [Online]. Available: http://www.cfd-online.com/Wiki/Solve_UV.f90_-_Solution_of_the_momentum_equations_for_U_and_V. [Accessed 28 12 2013].

[3] U. Ghia, K. N. Ghia and C. T. Shin, "High-Re Solutions for Incompressible Flow Using the Navier-Stokes Equations and a Multigrid Method," *Journal of Computational Physics,* no. 48, pp. 387-411, 1982.

Appendix A – PPW for 4th Order Central Difference

The fourth order central difference formula is found using four Taylor series expressions for u_{j+2}, u_{j+1}, u_{j-1}, u_{j-2} and combining them into the expression:$-(u_{j+2}) + 8(u_{j+1}) - 8(u_{j-1}) + (u_{j-2})$. Isolating $\frac{du}{dx}$ and simplifying this equation yields the following:

$$\frac{du}{dx} = \frac{-u_{j+2} + 8u_{j+1} - 8u_{j-1} + u_{j-2}}{12\Delta x}$$

Let $u_i = e^{ikx_j}$, where $x_j = j\Delta x$ and note that $\frac{de^{ikx}}{dx} = ike^{ikx}$. This results in:

$$\frac{du}{dx} = \frac{-e^{ik(j+2)\Delta x} + 8e^{ik(j+1)\Delta x} - 8e^{ik(j-1)\Delta x} + e^{ik(j-2)\Delta x}}{12\Delta x} = \frac{(-e^{2ik\Delta x} + 8e^{ik\Delta x} - 8e^{-ik\Delta x} + e^{-2ik\Delta x})e^{ikx_j}}{12\Delta x}$$

Since $e^{ikx} = \cos(kx) + i\sin(kx)$ then:

$$\frac{du}{dx} = \frac{(-[\cos(2k\Delta x) + i\sin(2k\Delta x)] + 8[\cos(k\Delta x) + i\sin(k\Delta x)] - 8[\cos(k\Delta x) - i\sin(k\Delta x)] + [\cos(2k\Delta x) - i\sin(2k\Delta x)])e^{ikx_j}}{12\Delta x}$$

$$\frac{du}{dx} = \frac{i[-\sin(2k\Delta x) + 8\sin(k\Delta x)]e^{ikx_j}}{6\Delta x} = ik^*e^{ikx}$$

$$k^* = \frac{-\sin(2k\Delta x) + 8\sin(k\Delta x)}{6\Delta x}$$

$$\frac{k^*}{k} = \frac{-\sin(2k\Delta x) + 8\sin(k\Delta x)}{6\Delta xk}$$

The error can be defined as:

$$\left|\frac{k^* - k}{k}\right| = \left|\frac{-\sin(2k\Delta x) + 8\sin(k\Delta x) - 6\Delta xk}{6\Delta xk}\right|$$

In order to have an error less than or equal to 0.1%:

$$\left|\frac{k^* - k}{k}\right| = \left|\frac{-\sin(2k\Delta x) + 8\sin(k\Delta x) - 6\Delta xk}{6\Delta xk}\right| \leq 0.001$$

PPW is defined as $n = \frac{2\pi}{k\Delta x}$, substituting $k\Delta x = \frac{2\pi}{n}$ gives:

$$\left|\frac{-\sin\left(\frac{4\pi}{n}\right) + 8\sin\left(\frac{2\pi}{n}\right) - 6\frac{2\pi}{n}}{6\frac{2\pi}{n}}\right| \leq 0.001$$

Solving for n gives a value of 15.01885. This means that PPW for fourth order central difference is 15 for an error $\leq$ 0.1%.

Appendix B – Modified QUICK Scheme

$$\frac{du}{dt} + a\frac{du}{dx} = 0$$

$$\frac{du}{dt} + a\frac{u_e - u_w}{\Delta x} = \frac{du}{dt} + a\frac{(6u_i + 3u_{i+1} - u_{i-1}) - (6u_{i-1} + 3u_i - u_{i-2})}{8\Delta x} = 0$$

$$\frac{du}{dt} + a\frac{(3u_i + 3u_{i+1} - 7u_{i-1} + u_{i-2})}{8\Delta x} = 0$$

The Taylor series expressions for $u_{i+1}, u_{i-1}, u_{i-2}$ are as follows:

$$u_{i+1} = u_i + \Delta x u' + \frac{1}{2}\Delta x^2 u'' + \frac{1}{6}\Delta x^3 u''' + \frac{1}{24}\Delta x^4 u''''$$

$$u_{i-1} = u_i - \Delta x u' + \frac{1}{2}\Delta x^2 u'' - \frac{1}{6}\Delta x^3 u''' + \frac{1}{24}\Delta x^4 u''''$$

$$u_{i-2} = u_i - 2\Delta x u' + 2\Delta x^2 u'' - \frac{4}{3}\Delta x^3 u''' + \frac{2}{3}\Delta x^4 u''''$$

Evaluating $3u_{i+1} - 7u_{i-1} + u_{i-2}$ using the left side of the above expressions yields:

$$3u_{i+1} - 7u_{i-1} + u_{i-2} = -3u_i + 8\Delta x\frac{du}{dx} + \frac{1}{3}\Delta x^3\frac{d^3u}{dx^3} + \frac{1}{2}\Delta x^4\frac{d^4u}{dx^4}$$

Rearranging the equation gives:

$$\frac{3u_i + 3u_{i+1} - 7u_{i-1} + u_{i-2}}{8\Delta x} = \frac{du}{dx} + \frac{1}{24}\Delta x^2\frac{d^3u}{dx^3} + \frac{1}{16}\Delta x^3\frac{d^4u}{dx^4}$$

Substitution into the original equation:

$$\frac{du}{dt} + a\left(\frac{du}{dx} + \frac{1}{24}\Delta x^2\frac{d^3u}{dx^3} + \frac{1}{16}\Delta x^3\frac{d^4u}{dx^4}\right) = 0$$

The modified equation for QUICK can then be written as:

$$\frac{du}{dt} + a\left(\frac{du}{dx}\right) = a\left(-\frac{1}{24}\Delta x^2\frac{d^3u}{dx^3} - \frac{1}{16}\Delta x^3\frac{d^4u}{dx^4} + \cdots\right)$$